Laser Guidance and Trapping of Mesoscale Particles in Hollow-Core Optical Fibers

Michael J. Renn,* Robert Pastel, and Heather J. Lewandowski
Department of Physics, Michigan Technological University, Houghton, Michigan 49931
(Received 16 April 1998)

Mesoscale particles are guided and trapped in micron-sized hollow optical fibers using a $\frac{1}{2}$-W near-infrared diode laser. The optical scattering force calculated using geometrical ray optics is 3×10^{-11} N for a 7-μm polystyrene sphere, and agrees well with velocity measurements of optically guided spheres in water. We have levitated a variety of particles using laser-fiber guidance, and have mixed micron-sized glycerin droplets in two-beam laser-fiber traps. [S0031-9007(99)08460-4]

PACS numbers: 79.60.Jv

Optical forces arising from scattered and refracted light at dielectric interfaces are powerful tools for manipulating small particles. Ashkin and collaborators [1,2] first demonstrated laser trapping of microscopic spheres and derived quantitative models of the optical forces. His single beam traps [3], optical tweezers, are widely used in biology for manipulating biological [4] and dielectric [5] particles. Applications are also found in aerosol science [6] and chemistry [7].

Laser guidance uses optical forces to both axially confine and propel particles along a laser beam. Many particles can be transported simultaneously over distances of microns to centimeters. The first demonstration of laser guidance used weakly focused beams to levitate particles [2,8]. The divergence of the Gaussian beams limited the transport distances to the Rayleigh length. Kawata and Sugiura demonstrated another laser guidance scheme utilizing scattering forces from evanescent waves [9]. Their technique is limited by the sixth power size dependence of Rayleigh scattering to larger particles.

Hollow-core optical fibers enhance the flexibility of laser guidance. In our apparatus, both the laser light and the particles are guided in the hollow-core region of the fiber. The laser light is guided in grazing-incidence modes, and the particles are guided and propelled by optical absorption, scattering, and gradient forces. The fiber walls control the transport environment by shielding the particles from the surrounding fluid motion. Fiber-assisted guidance can transport particles with a single laser beam and trap particles between counterpropagating beams.

Laser guidance in fibers was first demonstrated with Rb atoms [10]. In this Letter, we extend the technique to mesoscale solid particles and liquid droplets. Laser light, nonresonant with material transitions, is used to guide the particles at atmospheric pressure and room temperature. The particle sizes range from 50 nm to 10 μm and fiber inner diameters range from 10 to 50 μm. Requirements for guidance are the following: (1) The particle refractive index be larger than the surrounding fluid, assuring the gradient force is attractive towards high intensity; and (2) the optical guidance potential be greater than the thermal kinetic energy of the background molecules, preventing deflection of particles into the fiber wall.

The guiding optical fields are generated by focusing a laser beam at low numerical aperture into a hollow fiber. The lowest loss, grazing-incidence mode has radial ρ and axial z intensity dependence given by [11]

$$I(\rho, z) = I_0[J_0(\chi\rho)]^2 e^{-z/z_0}, \tag{1}$$

where $\chi \cong 2.4/\rho_0$, ρ_0 is the radius of the hollow region of the fiber, and I_0 is the field intensity at $\rho = 0$. The decay distance along the fiber is

$$z_0 = 6.8\,\frac{\rho_0^3}{\lambda^2}\,\frac{\sqrt{\nu^2 - 1}}{\nu^2 + 1}\,, \tag{2}$$

where ν is the ratio of the fiber-wall refractive index to the hollow region refractive index, and λ is the laser wavelength in the hollow region. The particle is confined by the radial intensity gradient force, and propelled axially by scattering and absorption forces. The axial gradient force is negligible.

The snapshots in Fig. 1 show the levitation of a 5-μm water droplet in a 5-mm curved section of air-filled fiber. A 240-mW laser beam ($\lambda = 800$ nm) is coupled with 90% efficiency into the lowest-loss mode. The 5-μm water droplets, estimated by optical microscopy, are funneled into the fiber by the laser light from a fog of droplets. The scattered light from the droplet is easily seen by the naked eye as the droplet travels through the fiber. The droplets can be deflected by at least 30° from straight trajectories. The deflection angle is limited by mode attenuation, which is inversely proportional to the fiber's radius of curvature squared and doubles for a 30° bend in a 2-cm fiber. Blocking the laser light causes the particle to attach to the wall, demonstrating that transport is without wall contact.

The optical forces exerted on dielectric particles with radius larger than the laser wavelength can be calculated using geometrical ray optics [5,12]. Figure 2 shows the radial dependence of the axial scattering and radial gradient forces on a 7-μm polystyrene sphere ($n_s = 1.59$) near the entrance of a *water*-filled fiber using geometric ray calculations [5,12] and Eq. (1) for the intensity

 0031-9007/99/82(7)/1574(4)$15.00

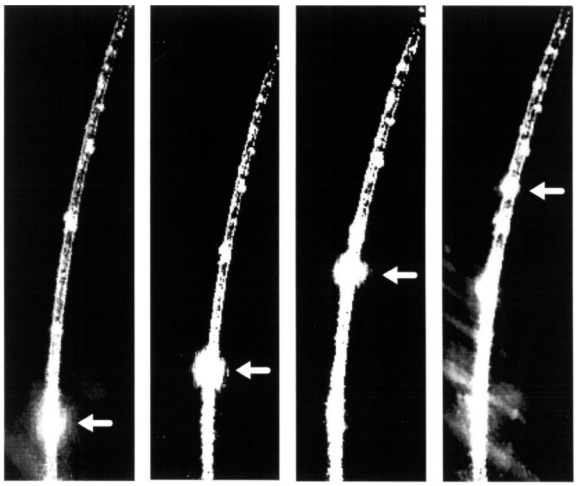

FIG. 1. Snapshots in time showing the levitation of a water droplet in a 30-μm, air-filled hollow fiber. In each snapshot, a 5-mm section of 20-mm long fiber is imaged on a CCD camera. The bright scattering of light by the droplet, indicated by the arrow, is easily seen by the naked eye as the water droplet travels upward through the curved region. Bending the fiber is accomplished by translating the output tip while holding the input end fixed.

profile. The calculated forces correspond to experimental conditions; a 3.6-mm laser beam diameter (measured between $1/e^2$ points), and a 240-mW laser beam coupled with 90% efficiency into a 20-μm fiber. The gradient force increases nearly linearly with small displacements from the fiber center indicating a restoring force drawing the particle to high intensity. Assuming the particle motion is damped to the radial center by the viscous background fluid, the radial confinement can be estimated from the radial potential of the restoring force. The potential depth is $U \sim \frac{1}{2}F_\rho \rho_0 = 1 \times 10^{-16}$ J, 4 orders of magnitude larger than the background fluid thermal energy, $k_B T = 4 \times 10^{-21}$ J. Equating the radial potential to the average background thermal energy, $U(\rho) = k_B T$, the estimated particle localization is 0.1 μm to the fiber center. The axial force is nearly constant for small displacements from the center, $F_z \sim 3 \times 10^{-11}$ N, and is over 2 orders of magnitude larger than the particle weight in water, $F_g \sim 9 \times 10^{-14}$ N.

Figure 3 shows the position with time of an optically guided 7-μm polystyrene sphere near the entrance of a 20-μm water-filled fiber. The slope of this curve, corresponding to particle velocity, abruptly decreases at the fiber entrance because of increased drag. The measured velocity immediately before and after the fiber entrance is 650 and 300 μm/s, respectively. The axial velocity is determined by Stokes' drag, $F_D = 6\pi\eta aKV$, where V is the particle velocity, η is the shear viscosity of the fluid, and a is the particle radius. K is a wall correction factor for low Reynolds number flow in the center of the fiber and is given to third order in particle size by [13]

$$K = \left[1 - 2.1\left(\frac{a}{\rho_0}\right) + 2.1\left(\frac{a}{\rho_0}\right)^3\right]^{-1}.$$

The increased drag due to the proximity of the fiber wall lowers the velocity compared to the velocity outside the fiber. The calculated velocities using geometric ray calculations [12] and Stokes' drag are 600 and 230 μm/s just outside and inside the fiber; giving good agreement with measured velocities. Convective fluid motion can contribute to the discrepancy, but is minimized by positioning the fiber output near a surface.

Besides water droplets and polystyrene spheres, we have guided glycerin droplets, salt, sugar, KI, CdTe, Si, and Ge crystals, and Au and Ag metal particles with sizes ranging from 50 nm to 10 μm using a 0.5-W laser and 17-μm-inner-diameter air-filled fibers. The behavior of the metals is similar to that of dielectric particles except optical absorption adds to the propulsion force and can melt the particle. We have observed axial velocities of order 1 cm/s for micron-sized Ag in air-filled fiber.

Of particular interest for direct-write applications [14] is the smallest particle size that can be guided. When the particle diameter is much smaller than the wavelength of light, the optical forces are predicted by Rayleigh

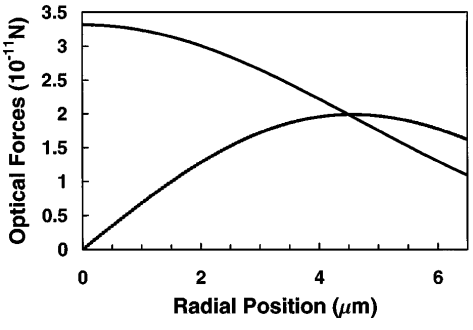

FIG. 2. Calculated radial (jagged curve) and axial (solid curve) optical forces on a 7.0-μm polystyrene latex sphere near the entrance to a 20-μm water-filled fiber. The 220-mW laser beam is coupled into the lowest-loss fiber mode.

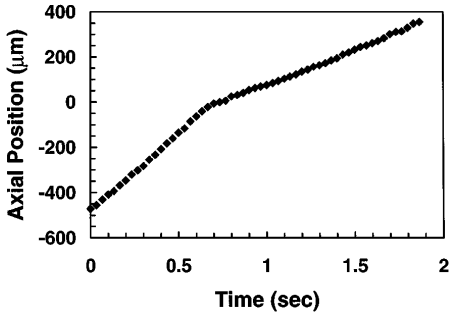

FIG. 3. Measurements of axial position with time of a 7-μm diameter polystyrene sphere optically guided from bulk fluid into a 20-μm diameter fiber. The position $z = 0$ corresponds to the fiber input tip. The particle velocity (slope of curve) abruptly decreases when the sphere enters the fiber as a result of increased drag.

scattering theory [15]. The radial optical potential is then

$$U = -\frac{n_b}{2c}\,\alpha I = -\frac{n_b^3 a^3}{2c}\left(\frac{m^2 - 1}{m^2 + 2}\right) I\,,$$

where α is the particle polarizability, I is the peak intensity, m is the ratio of the particle refractive index n_s to the background index n_b, and c is the speed of light. Assuming an air-filled fiber ($n_b = 1.0$) and an achievable laser intensity of 10^{12} W/m^2, the potential energy is comparable to $k_B T$ when the particle diameter $2a$ is 20 nm ($n_s = 1.59$). High refractive index and metal particles have deeper confinement potential energy, and their minimum particle size reduces by the cube root of the potential depth. Tapered fibers can potentially enhance confinement over short distances.

Large particle flux is essential for direct writing [14]. Since the optical guidance field extends along the length of the fiber, many particles can be guided simultaneously. We have observed particle flux exceeding 10^2 s^{-1} for 100-nm polystyrene spheres in 20-μm water-filled fiber using a 500-mW laser. The particles flow evenly spaced "single file" with a 100-μm/s velocity, measured from video microscopy. The small particles are interacting as coherent dipoles [16] and separate themselves by a distance λ. At high particle flux, fluid entrainment and particle interactions strongly influence the velocity; consequently, single particle force calculations are invalid.

The dominating effect determining the maximum guidance distance is the optical intensity decay along the fiber. Using Eq. (2), the exponential decay length for a 20-μm fiber is $z_0 = 7.6$ mm. Particles are typically guided several decay lengths in the fiber while, for laser guidance without fibers, strong confinement is limited to approximately the Rayleigh distance, 10^{-4} m for a 20-μm laser spot size. Although z_0 limits the overall guidance distance, the attenuation can be used to construct traps. A single beam trap is formed by balancing the gravitational and axial scattering forces in a vertically oriented fiber. The levitation height is $z = z_0 \log(F_0/F_g)$, where F_0 is the axial force at the fiber entrance, and F_g is the gravitational force. Figure 4 shows experimentally the dependence of levitation height on laser power for a single 1-μm sugar crystal in a 20-μm *air*-filled fiber. The crystals are formed by evaporation of water-sugar droplets, the water evaporates during levitation leaving the solid crystal. We observe stable levitation for more than 5 hours. The solid curve is the calculated logarithmic dependence of levitation using $z_0 = 7.6$ mm and is normalized to the lowest data point. One application of this single beam trap is a mass scale similar to the apparatus proposed by Ashkin [17]. Specifically, a mass change of one part in 10^4 will produce an 1-μm displacement in a 20-μm-inner-diameter fiber. The mass resolution is dependent on z_0 and can be adjusted using different sizes of fibers. Optical feedback stabilization should allow the measurements to be performed in vacuum [17].

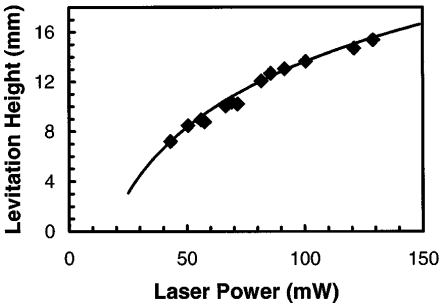

FIG. 4. Measured (diamonds) and calculated (solid curve) levitation height versus laser power of a single 1-μm sugar crystal in a vertically oriented 20-μm fiber. The solid curve uses a calculated attenuation, $z_0 = 7.6$ mm, and is normalized to the first data point.

We have constructed a second trap using counterpropagating laser beams coupled into opposite ends of a horizontal fiber. This trap is similar to the trap of Constable *et al.* [18] in that at the trap center the scattering forces cancel and the radial forces double. Using Eq. (1), the intensity profile within the fiber is given by

$$I(\rho, z) = 2I_0 \exp\left(-\frac{l}{z_0}\right) J_0^2(\chi\rho) \cosh\left(\frac{z - l}{z_0}\right),$$

where $2l$ is the fiber length, and I_0 is the laser intensity at the fiber ends. Using calculations similar to Fig. 2 and assuming $z_0 = 7.6$ mm, $l = 7.6$ mm, the radial spring constant for a 7-μm polystyrene sphere in air is $k_\rho = 4.6 \times 10^{-6}$ N/m, and the axial spring constant is $k_z = 3.2 \times 10^{-9}$ N/m. Because $k_\rho \gg k_z$ and the trap is overdamped, the particle motion is predominately one-dimensional Brownian. We have trapped glycerin droplets, salt crystals, and metal particles ranging in size from 50 nm to 5 μm in this configuration for many hours.

The two-beam trap can be used for studying collisions and reactions of femtoliter droplets in controlled environments. Figure 5 shows the scattered intensity of 1- and 5-μm glycerin droplet collision with time. The scattered light is collected with a 0.25 numerical aperture microscope objective at 90° to the fiber, and detected with a photodiode. Before the collision, the total scattered light is the sum of the scattered light from the two droplets. After coalescence, the surface area of the combined droplet is not appreciably different from the larger droplet before the collision, and the total scattered light decreases. The intensity fluctuations just before the collision are likely caused by interference from approaching coherent dipoles [19]. The coalescent time, measured between 90% and 10% maximum intensity, is approximately 100 μsec. This trap may be used as a containerless microchemical reactor by mixing femtoliter chemicals and observing reaction dynamics via fluorescence emission and morphology dependent scattering.

In conclusion, optical guidance and trapping of microscopic particles in both air- and liquid-filled fibers has been

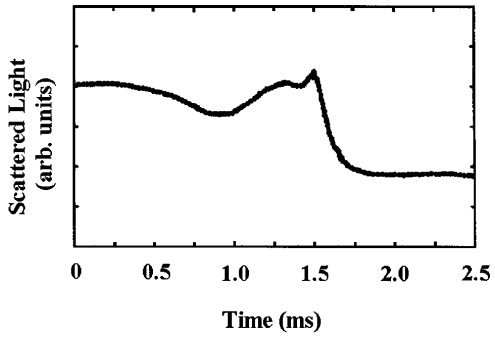

FIG. 5. Oscilloscope time trace of the light scattered about 90° from two glycerin droplets during a collision. At the beginning of the trace, two droplets, 1 and 5 μm in size, are each scattering light. The coalesced droplet scatters less light than the sum of the individual droplets. Consequently, the coalescence event is observable as a sharp decrease of scattered light. The coalescence time, estimated between 90% to 10% intensity points, is 100 μs. The oscillations in scattered light are characteristic of interfering coherent dipoles.

demonstrated. The laser guidance technique is flexible in the variety of particle types that can be manipulated and the trajectories over which they are guided. In addition to dielectric spheres, we have guided metal, semiconductor, and biological particles, as well as particles with nonspherical shape. We expect laser-fiber guidance will find applications in interdisciplinary areas such as aerosol particle trapping, biochemistry, direct writing of materials, and microfluidics.

This work was partially supported by Oak Ridge Associated Universities (Contract No. 970206).

*Corresponding author.
Electronic address: mrenn@mtu.edu

[1] A. Ashkin, Phys. Rev. Lett. **24**, 156 (1970).
[2] A. Ashkin and J. M. Dziedzic, Appl. Phys. Lett. **19**, 283 (1971).
[3] A. Ashkin, J. M. Dziedzic, J. E. Borkholm, and S. Chu, Opt. Lett. **11**, 288 (1986).
[4] K. Svoboda and S. M. Block, Annu. Rev. Biophys. Biomol. Struct. **23**, 247 (1994).
[5] A. Ashkin, Biophys. J. **61**, 569 (1992).
[6] A. Ashkin and J. J. Dziedzic, Science **187**, 1073 (1975).
[7] H. Misawa, N. Kitamura, and H. Masuhara, J. Am. Chem. Soc. **113**, 7859 (1991).
[8] T. N. Buican *et al.*, Appl. Opt. **26**, 5311 (1987).
[9] S. Kawata and T. Sugiura, Opt. Lett. **17**, 772 (1992).
[10] M. J. Renn *et al.*, Phys. Rev. Lett. **75**, 3253 (1995).
[11] E. A. Marcatile and R. A. Schmeltzer, Bell Syst. Tech. J. **43**, 1783 (1964).
[12] G. Roosen and C. Imbert, Phys. Lett. **59A**, 6 (1976).
[13] J. Happel and H. Brenner, *Low Reynolds Number Hydrodynamics* (Prentice-Hall, Englewood Cliffs, NJ, 1965).
[14] M. J. Renn and R. Pastel, J. Vac. Sci. Technol. B **16**, 3859 (1998).
[15] M. Kerker, *The Scattering of Light* (Academic, New York, 1969).
[16] M. M. Burns, J. M. Fournier, and J. A. Golovchendo, Phys. Rev. Lett. **63**, 1233 (1989).
[17] A. Ashkin and J. M. Dziedzic, Appl. Phys. Lett. **30**, 202 (1977).
[18] A. Constable, J. Kim, J. Mervis, F. Zarinetchi, and M. Prentiss, Opt. Lett. **21**, 1867 (1993).
[19] G. W. Kattawar and T. J. Humphreys, in *Light Scattering by Irregularly Shaped Particles*, edited by D. W. Schuerman (Plenum Press, New York, 1980)